ARQII Publication
http://arqiipubl.com/ams
APPLICATIONS OF
MODELLING AND SIMULATION
eISSN 2600-8084
VOL 8, 2024, 146-161

A CFD Analysis of the Effective Plume-Chimney Height of Lazy Plumes and its Implications to Clear Air Turbulence

C. -K. Too and C. -M. Chu*

Faculty of Engineering, Universiti Malaysia Sabah, 88400 Kota Kinabalu, Sabah, Malaysia

*Corresponding author: chrischu@ums.edu.my

Submitted 29 December 2023, Revised 17 April 2024, Accepted 21 April 2024, Available online 05 June 2024.

Abstract: Plume chimney is a plume that has chimney characteristics due to stack effects of plumes. In this study, Computational Fluid Dynamic (CFD) simulation was carried out for three different heights of chimney and three different diameters of chimney at various heat loads to cover a range of source Richardson number from 0.034 to 0.33, and plume function from 1.01 to 7.16. Reynold's average Navier-Stokes's conservation equations were solved in modelling the plume. A zero-gravity forced convection plume model was applied to obtain the overall total pressure drop. Effective Plume-Chimney Height (EPCH) was correlated with several parameters to obtain an empirical correlation. It was found that EPCH was related to the square root diameter of the chimney, as predicted by dimensional analysis in a pioneering plume rise study and concurred with all existing prediction methods. Through this finding, a scaling formula for plume characteristic height is proposed. The power indices of volumetric coefficient of expansion, temperature differences, mean density of plume source density difference of air between ambient and plume source were 0.45, 0,80, 1.09 and -0.97 respectively; and correlation with the air velocity was negligible. The EPCH predicted by the correlation derived using the current method was found to be very close to previous correlations at the same Richardson number and plume function. For improved applicability, the range of parameters should be sufficiently broad and evenly distributed in future analysis. The theory of effective plume-chimney height is strongly supported by this CFD analysis, in addition to experimental data from industrial tests. Implications of the phenomenon of effective plume-chimney height, where a lazy plume has invisible walls causing a stack effect, generates a sizeable up thrust that is recommended to be investigated as it may be one of several factors contributing to mesoscale Clear Air Turbulence phenomenon experienced by aircrafts.

Keywords: Clear air turbulence; CFD; Correlation; Effective plume-chimney height; Plume-chimney; Plume function; Richardson number.

1. INTRODUCTION

Plumes are omnipresent in our daily, natural or man-made environment. In natural environment, the most common examples are the ash plumes forming a huge particle-laden cloud from an erupting volcano and the vapour plumes above the forest fire. Man-made plumes above the industry smokestacks are common to the society. For the aviation industry clear air turbulence (CAT) [1][2] has been recognised as not originating from jet streams or crosswinds, as they were discovered in 1940's to occur even under perfectly calm and cloudless surroundings at high altitudes, defined as aircraft turbulence at above 5.6 km height whether cloud-free or within stratiform clouds. This calmness and cloudlessness fits into the condition where plumes occur and with climate change it is worth investigating any possible link between pockets of plumes of large source-area at mesoscale scale and clear air turbulence [3].

Plumes are classified into different types such as pure plume, flow driven by buoyancy effect; pure jets, flow driven by momentum; forced plume or jet, flow driven by both momentum and buoyancy effect [4]; Gaussian plume, flow that follow Gaussian distribution with a bell-shaped symmetry [5]; and converging or lazy plumes, flow that have high buoyancy flux relative to momentum flux [6][7]. Lazy plumes have only been studied in detail recently. Numerical simulation studies have been few and experimental studies are even fewer with the latest published article in 2018 [8] and the previous one in 2009 [9]. New grounds have been achieved in modelling near-field lazy plume entrainment behaviour [10][11][12].

In this study, the focus is on the stack effect of plumes with large Richardson number, or lazy plumes driven by natural convection. In contrast with forced convection, natural convection is a process in which heat is transferred within a fluid by the movement of fluid itself due to density gradient. The stack effect occurs at or near the plume source. This movement of air is caused by the air buoyancy as a result of the density differences due to temperature differences or moisture differences. The hydraulic balance of a chimney is normally over its wall height which is a solid boundary. A plume-chimney has no solid

boundary as its chimney wall, and therefore a chimney with a significant magnitude of EPCH in comparison to its solid chimney wall will have an effective chimney height in excess of its solid wall. The buoyancy pressure of this excess height can be estimated by the difference between the measured pressure loss of the natural convection flow through the chimney and the solid chimney height buoyancy pressure (Figure 1). An important assumption is that the pressure loss due to the lazy plume is much less than that of the pressure loss through the solid chimney.

However, it is difficult to obtain accurate natural convection data experimentally using air as the test fluid where the velocity is below the lowest of an instrument's range and not realistic to conduct in terms of scale and budget. Hence, Computational Fluid Dynamics (CFD) simulation is a preferred option for a high-accuracy estimation of the effective plume-chimney height. A special technique in deducing the effective plume-chimney height is described in detail.

Plume-chimney characteristics are important to indicate the effectiveness of equipment such as air-cooled heat exchanger operating in natural convection mode, a concept which was first propounded by Doyle and Benkly [13]. Previous studies [25] had shown that a set of data obtained at an industrial-scale air-cooled heat exchanger appeared to be reasonably predicted by an equation derived from established empirical correlations. Rather than conducting full-scale industrial experiments using air to validate the correlation, which would be expensive due to the scale of the test facility when altering its design for experiments, it was decided to simulate the plume-chimney to derive a correlation with similar parameters from the data analysis.

The objectives of this study are:

1. To derive an effective plume-chimney height empirical correlation by CFD simulation using Phoenics VR.
2. To study the behaviour of effective plume-chimney height against plume function and source Richardson number.

The scope of work was to simulate and analyse the effective plume-chimney height at heights of 3, 5, 10 m chimney, heating loads of 10 to 1500 kW and diameters of heating source ranging from 0.5, 1.0, 2.0 and 5.0 m resulting in Richardson numbers of 0.034 to 0.33. A possible link between the zone of flow establishment (ZFE) of plume-chimney and CAT [1], which is important to the aviation industry because of safety concern for the passengers [14], are briefly discussed for future investigation, since it will be beyond the scope of this study to discuss in-depth the role of plume-chimney, if any, in CAT.

2. THEORETICAL BASIS

2.1 Entrainment Coefficient

Entrainment coefficient was first introduced by Morton, Taylor and Turner [15] as shown in Equation (1),

$$r = \frac{6\alpha}{5} z \tag{1}$$

with the assumption made that α was a constant entrainment coefficient and equations developed for local fluxes of buoyancy, momentum and volume in an axisymmetric turbulent plume that assumed the Boussinesq approximation. The entrainment coefficient, α, according to Morton *et al.* [15] can then be estimated by measuring the plume radius. With the considerations of non-zero values of source volume flux, buoyancy flux and momentum flux, Morton [16] extended the work, achieved with forced plumes with an excess momentum at the sources. This work was further extended with the indication of local point of interest in a plume as the source parameter defined at source $z = 0$ on scale diagrams [17].

$$\Gamma(z = 0) = \Gamma_0 = \frac{5Q_0^2 F_0}{4\alpha M_0^{2.5}} \tag{2}$$

The identification of lazy plumes and forced plumes based on balance of fluxes at the source can be achieved through Equation (2) where Q_0 is the mass flux, F_0 is buoyancy flux and M_0 is momentum flux. The plumes are to be classified into lazy plumes (Γ>1), pure plumes (Γ=1) and forced plumes (Γ<1) Lazy plumes have also been called distributed plumes [7]. However, the term 'lazy' is preferable with the meaning of reduced forces whereas 'distributed' means the source can be lazy, pure, or forced.

The assumption of Morton *et al.* [15] where the entrainment coefficient, α is independent of height has been challenged by several authors. List and Imberger [18] contented that with α maintained as constant when modelling forced plumes would overestimate the radial growth rate due to the entrainment in a jet being relatively lower than in a pure plume. Bhat and Narasimha [19] also argued that it would overestimate the volumetric flux in clouds due to the increase in plume buoyancy flux as latent heat released. In their findings, Sreenivas and Prasad [20] estimated a reduced α value where off source heating and acceleration of plumes were applied. Several workers [21][22] also proposed similar argument where α is a function of self-similarity drift, the rate of change of relative radii of velocity and buoyancy profiles. Lazy plumes are achieved through these Richardson-number-dependent models as for achieving large α leads to a large Richardson number. The correlation of Richardson number and α is shown in Equation (3):

$$\alpha = a_1 + a_2 R_i \tag{3}$$

where R_i is the Richardson number, and $a_1 > 0, a_2 > 0$ at source is:

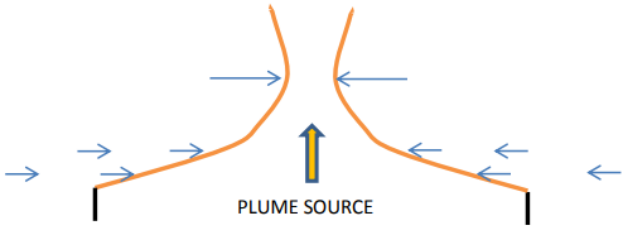

Figure 1. Lazy plume rising from large source area.

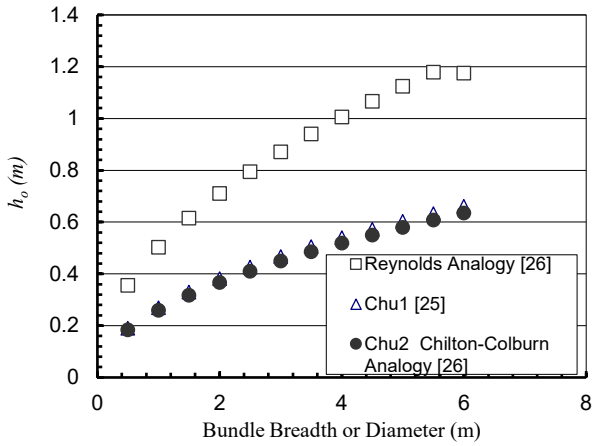

Figure 2. Effect of bundle breadth or diameter on EPCH for three methods.

$$Ri_0 = \frac{r_0 g(\rho_a - \rho_0)}{\rho_0 w_0^2} \tag{4}$$

Hunt and Kaye [23] re-cast the conservation equations of Morton *et al.* [15], where α was expressed in terms of plume radius, local balance momentum, and initial flux gain with height, and established expressions for the minimum plume radius and neck height of lazy plumes. They formulated and examined the near-source region of lazy plumes from horizontal area source and established the power law behaviour for buoyancy flux, volume flux, momentum flux, and vertical velocity. They suggested that α could be a constant for several reduced entrainment flow but not for all plume flows. Later Ciriello and Hunt [10] went on to analyse area source plumes using the virtual origin approach, thereby determining the coefficients of a variable entrainment function, which indicates that a larger entrainment rate is expected near the source of lazy plumes, and so does not contradict our proposal for a plume-chimney theory. Their variable entrainment function was based on Carazzo *et al.*'s [24] using Richardson number as the controlling parameter, which is necessary but insufficient to describe the near-field plume behaviour.

Hunt and Kaye's findings showed a zero-entrainment region at near source, confirmed by simulation of plumes from very lazy (high plume function) to forced plumes [11], where the entrainment coefficient based on 'top hat' definition of Morton *et al.* [15] began at zero at height $Z = 0$ form the source, rising rapidly then reduced gradually to asymptotic value of pure plume (See Figure 6 of their paper). This behaviour suggests an entrainment flow that is a main flow rather than a secondary one with streamlines that are nearly horizontal above a finite source. This creates a core region in the centre of the plume that is not fully entrained to dilute its buoyancy as found in pure plumes. This incomplete dilution results in a buoyant core region that is demonstrated by a centreline temperature remaining constant for a vertical distance until the necking point. It is this invisible plume wall that can be exploited for stack effect.

2.2 Effective Plume-Chimney Height

Doyle and Benkly [13] introduced the concept of "Effective Plume Height" for lazy plumes (Figure 1) based on atmospheric plume rise dimensional analysis that characteristic heights of plumes are proportional to the 1/4th power of buoyancy flux [15] or the square root of source diameter and defined it as

$$h_o = \frac{\int_{h=0}^{h=h_{max}} \rho dh}{\rho_o} \tag{5}$$

This height was later renamed as effective plume-chimney height (EPCH) [25]. Intuitively, to reckon the entire plume column up to the maximum height driving the draft through the source is not feasible. They presented empirical formulae to evaluate heat loads of air-cooled heat exchangers attainable in the event of power outage or under fanless operations. Chu [25] discusses the derivation of a power-law equation from thermo-mechanical considerations and using established heat transfer correlations only. The equation predicts that the effective plume-chimney height depends on the square root of bundle breath or diameter, L_B, and a function of the temperature difference ΔT, outlet temperature T, density difference $\Delta\rho$ and dynamic viscosity but suggests independence of the draught for full-sized heat exchangers. The equation for laminar flow where $Gr.Pr < 10^9$ was also presented. Further derivations of the effective plume-chimney height were done based on Reynolds Analogies and Chilton-Colburn analogies [26]. The graph of effect of bundle breadth or diameter on EPCH for three methods is shown as in Figure 2, which agree with Doyle and Benkly [13] that the index is 0.5. These were developed based on empirical correlations of limited parametric variations. A rigorous derivation by numerical simulation based on Navier-Stokes equations of conservation using a computational fluid dynamics software would strengthen the validity of the equations and extend the range of applicability, which will be useful for design.

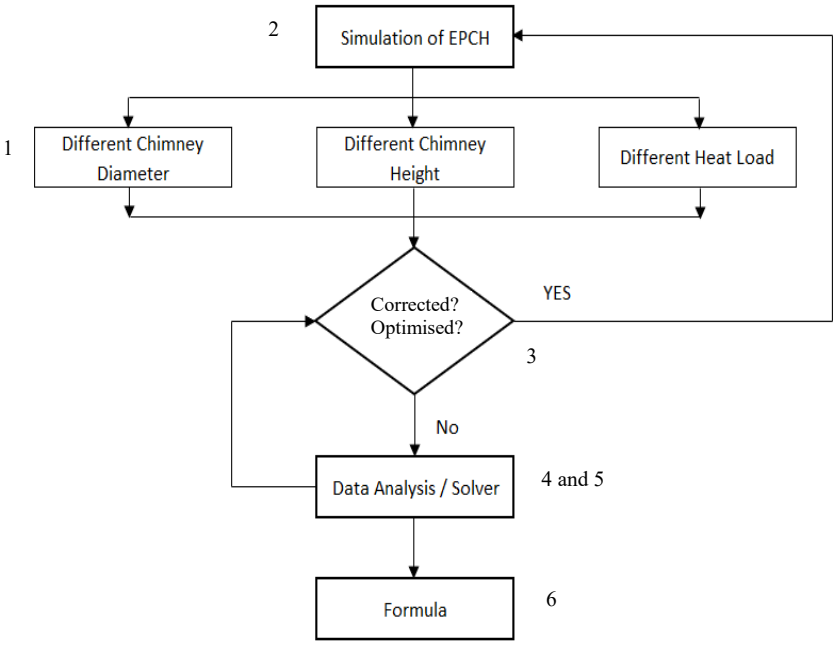

Figure 3. Methodology flow chart.

3. METHODOLOGY

The approach of this paper was to use simulation where it is virtually impossible to achieve a condition by real experiments: the setting of a zero-gravity for a heated air flow to determine its pressure losses by matching the outlet temperature of the buoyant flow. The steps are listed as following and depicted in Figure 3:

1. The simulation of condition with different diameter of cylinder, different height of cylinder and different heat load is simulated using Phoenics VR.
2. The settings are as listed in Section 3.4.
3. The mesh grid is optimised by the criterion of mass flow rate.
4. The EPCH of different conditions are determined and recorded.
5. The results are analysed to obtain the correlation between EPCH and other parameters.
6. The formula of EPCH empirical correlation is obtained.

3.1 EPCH Determination

Vertical cylinders (chimney) in four different diameters size and four different heights with heated air flowing through were selected as the simulation models. Reasonable assumption of $\pm 0.1\%$ of heat load and $\pm 7\%$ of air mass flowrate was applied for the validation of flow through a vertical cylinder by natural convection [27]. The total frictional loss of a natural draft chimney system is balanced by the total buoyancy head [28]. Hence, EPCH can be determined by subtracting the solid column buoyancy head from the total resistance head. The balance is as shown in Equation (6):

$$[h_o(\rho_a - \rho_o) + h_{sw}(\rho_a - \rho_{av})] = \Delta p_{pipe} + \Delta p_{inlet} + \Delta p_{outlet} \quad (6)$$

In the previous CFD analysis on 3 m to 50 m high chimneys at a constant 2 m diameter [27], it was found that if the Δp_{pipe} was estimated by applying Haaland [29] equation for Darcy friction factor, where Δp_{inlet} and Δp_{outlet} were estimated by ASHRAE [30] *K*-coefficients for air pipes and ducts, by setting the *K*-coefficient for sharp entrance effect at 0.38 and outlet sudden expansion at 1.0, the pressure drop equation did not balance, possibly due to the over-estimation of the entrance contraction and outlet expansion losses. The table comparing the methods of calculating EPCH from CFD simulation results is reproduced here, with predictions shown alongside for reference.

The total pressure drops in Table 1 (column g) estimated by summing the pipe wall, inlet and outlet losses was grossly higher than that estimated by the CFD using the value of a compressor generated-pressure to move the air at the same averaged outlet temperature and flowrate as the natural convection chimney, as the EPCH (m) is much higher than the other methods of estimations. This supports the use of obtaining the overall pressure drop through the natural draft chimney by applying the method of matching a zero-gravity forced convection heated flow with the natural draft (ND) buoyant flow. Experimental measurements of pressure losses in natural convection is extremely difficult as it necessarily intrudes into the flow.

Table 1. Comparison between EPCH calculated from friction factor and *K*-coefficients from CFD where Chu's previous correlations are placed alongside as reference.

(a) h_{sw} (m)	(b) Reynolds number	(c) Pipe Pressure Drop (Pa)	(d) Sudden Contraction Loss (Pa)	(e) Sudden Expansion Loss (Pa)	(f) Solid-Walled Chimney Buoyant Pressure (Pa)	(g) ΔP equation EPCH (m)	(h) ND-0G CFD EPCH (m)	Prediction	
								(i) Chu1 [25]	(j) Chu2 [26]
3	159792	0.03	0.83	2.48	2.12	0.92	0.26	0.46	0.41
10	263242	0.23	2.26	6.65	6.45	2.21	0.27	0.48	0.42
20	357563	0.81	4.17	12.27	12.66	3.76	0.35	0.48	0.42
50	539535	4.26	9.48	27.86	31.48	8.48	0.49	0.48	0.42

To alleviate the ill-defined locations of natural convection pressure loss measurements whether in experiments or in a CFD simulation, it was decided to determine the total buoyancy head (LHS of Equation (6)) of the column operating under natural convection by applying forced convection to the same column with the same flow rate and thermal load of natural convection as shown in Equation (7):

$$\Delta p_{compressor} = \Delta p_{pipe} + \Delta p_{inlet} + \Delta p_{outlet} \tag{7}$$

The pressure head produced by the compressor must be adjusted through trial and error to match the flow rate and the cylinder outlet temperature. Therefore, this method achieves partial similarity between plume and jet: thermal and dynamic similarity in a solid-walled chimney, and partial dynamic similarity between plume and jet as Reynolds number only applies to jets whereas plumes are influenced by both Richardson number and Reynolds number. Similar to the heater, compressor is set to occupy the entire inner column. This is because any smaller size was found to cause the air to form recirculation vortices in it. The natural convection mode of the plume will be driven by buoyancy in the normal way, while operating in the forced convection mode by using the compressor will make the plume purely driven by momentum. This process produces complete heat, inertia, and friction loss equivalents in the near-field region of the buoyancy-driven plume and momentum-driven jet. The friction loss that the compressor must overcome in the jet box is considered to be on the lower side of the plume value, because at almost the same speed, the friction loss due to the momentum entrainment of the jet has no buoyancy effect, so it is less than the sum of buoyancy and entrainment driven by momentum, and the deduced EPCH would also be lower than the actual value.

The structured mesh grid is used to directly solve the Reynolds average Navier-Stokes equation and run on Phoenics VR. The mesh grid is optimised with double of the default densities based on mass flowrate. Chen and Kim [31] turbulence model is used.

3.2 Convergence

As the plume-chimney is a natural convection system, the plume inlet velocity is not set, but by setting the heat load and the CFD software Phoenics would calculate the chimney exit temperature and velocity. The global convergence criterion was set as ±0.01%. The monitoring probe is located at above the top of the cylinder exit, obtaining temperature and velocity data. By using a SIMPLE technique, the Reynolds average Navier-Stokes conservation equations representing the computational domain were discretised and solved in steady state mode. The walls of the domain were frictionless by default. At the boundary of both top and bottom end of the domain objects were placed to allow for flow driven by pressure differences which is the mode of natural convection. All the simulations are simulated in steady state.

3.3 Assumptions

The assumptions of simulation are:

1. The domain material was an incompressible ideal gas.
2. No heat loss from the heating source through the chimney wall.
3. The chimney (cylinder) wall thickness was negligible (zero).
4. Normal wall function was applied.
5. Density variation of the fluid was applied.
6. Heating was uniformly distributed throughout the interior of the chimney.
7. No friction was caused by the compressor in the zero-gravity environment.
8. The chimney (cylinder) was symmetric at all points of circumference.

3.4 CFD Simulation Settings

The settings of the simulations are:

1. The diameter of the vertical cylinder was set at 0.5 m, 1 m, 2 m, and 5 m.
2. The height of the cylinder was set at 3 m, 5 m, and 10 m.
3. The plume outlet temperature was set as in solar chimney plumes with temperature ranging from 50℃ to 70℃ by manipulating the heat load.
4. Ambient temperature was 30°C and atmospheric pressure was at 101325 Pa.
5. Navier-Stokes conservation equations formed the mathematical fluid dynamics model.
6. Chen and Kim [31] was used as the turbulence model.

7. Global convergence criterion was set as $\pm 0.01\%$
8. CFD software used was Phoenics VR 2019 version.

3.5 Validation

The computational domain, mesh grid, geometry shapes and dimensions, pressure, temperature, velocity and energy input were essentially set in similar fashion as the plume simulation in [27], and the resulting Gaussian entrainment coefficients were between 0.091 – 0.113, close to Ciriello and Hunt's [10] list of past experimental and numerical studies with values of 0.073 – 0.110 and Nakagome and Hirata's [32] value of 0.112, and well within Carazzo *et al.*'s [24] range of 0.05 – 0.16 for Gaussian- profiled plumes. The current CFD simulation set up is therefore valid.

3.6 Preliminary Results

An initial test run for CFD simulation via Phoenics VR is conducted with 5 m height, 2 m diameter and 250 kW heat load. Figure 4 show the CFD simulation geometry for chimney, heater (heating source) and measurement sections for all case. The mesh grid optimisation of this test run is listed in Table 2. The results for pressure, temperature and velocity profile for this simulation are shown in Figure 5 to Figure 7.

The temperature results data for each section are tabulated in Table 3. Section I represents the inlet section of the chimney at (z = 0.5 m) and section O represents the outlet section of the chimney at (z = 5.5 m). The deviation between the simple average and the trapezium average appears negligible, at less than 0.1 per cent, showing that the temperature rise was reasonably linear. The temperature contour profile in Figure 6 indicates that no flow reversal (cold inflow) occurred at the outlet. With trapezium average temperature data, the average heated density, ρ_{av} was calculated as 1.0963 kg/m^3 using Equation (8). The ambient air density, ρ_a was calculated as 1.1664 kg/m^3 using Equation (8) at ambient temperature of 30°C. The Solid-walled Buoyant Pressure, Δp_{sw} was calculated as 3.44 Pa and compressor-generated pressure, $\Delta p_{compressor}$ as 3.79 Pa using Equations (9) and (10) respectively, where F was the force in N specified for the compressor.

$$\Delta p_{sw} = h_{sw}(\rho_a - \rho_{av})g \tag{9}$$

$$\Delta p_{compressor} = \frac{4F}{\pi d^2} \tag{10}$$

Table 2. Structured mesh grid optimisation for test run model.

Model	Mesh grid density by number of cells in region
6.28 rad × 5 m × 2 m diameter Heat Load: 250 kW	X: 1; Y: 4, 36; Z: 2, 2, 2, 2, 2, 2, 2, 2, 2, 2, 2, 2, 30, 26

X: Angular dimension, Y: Radial dimension, Z: Vertical dimension.

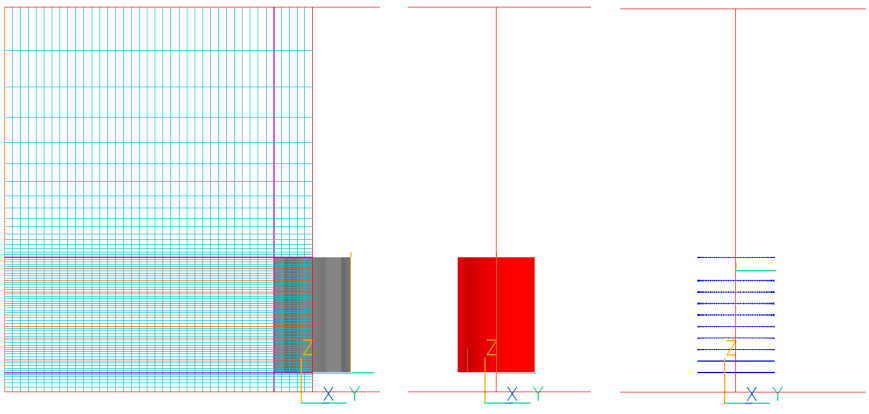

(a) Structured Mesh Grid (b) Heater size (c) Measurement section

Figure 4. CFD simulation geometry for chimney, heater and measurement sections.

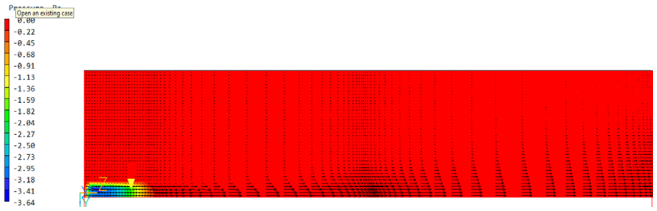

Figure 5. Plume pressure profile of 5 m × 2 m diameter, 250 kW simulation.

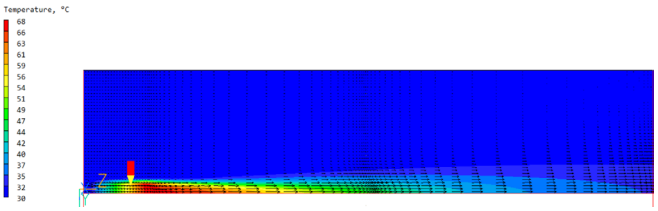

Figure 6. Plume temperature profile of 5 m × 2 m diameter, 250 kW simulation

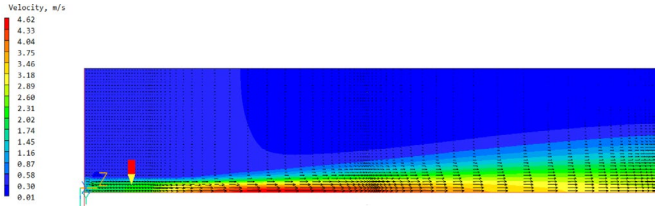

Figure 7. Plume velocity profile of 5 m × 2 m diameter, 250 kW simulation.

Table 3. Sectional temperature data of 5 m × 2 m diameter, 250 kW simulation.

Section	Temperature (°C)	Section	Temperature (°C)
I	30.95	7	49.44
O	66.91	8	53.13
3	34.67	9	56.83
4	38.37	10	60.53
5	42.06	11	64.23
6	45.75	Simple Average	49.35
Trapezium Average		49.39	

Table 4. Simulation condition.

Case	Chimney diameter (m)	Chimney height (m)	Heat load (kW)	Outlet plume temperature (°C)	Case	Chimney diameter (m)	Chimney Height (m)	Heat Load (kW)	Outlet Plume Temperature (°C)
1	0.5	3.0	10	59.56	9	2.0	3.0	200	65.84
2	0.5	5.0	10	56.61	10	2.0	5.0	150	55.94
3	1.0	3.0	50	65.40	11	2.0	5.0	200	61.76
4	1.0	5.0	50	61.43	12	2.0	10.0	250	58.95
5	1.0	10.0	50	54.60	13	5.0	5.0	750	51.61
6	1.0	10.0	75	62.73	14	5.0	5.0	1000	56.40
7	2.0	3.0	100	52.00	15	5.0	10.0	1250	55.75
8	2.0	3.0	150	59.23	16	5.0	10.0	1500	59.25

The EPCH, h_0 is calculated as 1.040 m using Equation (11):

$$h_0 = \frac{\Delta p_{compressor} - \Delta p_{sw}}{(\rho_a - \rho_o)g} \tag{11}$$

3.7 Simulation Condition

The outlet plume temperature was designed to be ranging from 50°C to 70°C as specified in Section 3.4 typical of solar chimneys. 16 different scenarios fulfil the specification are determined and tabulated in Table 4. The simulated outlet plume temperature for these 16 scenarios ranged from 51.61°C to 65.84°C. The mesh grid optimisation of each case is as listed in Table A1 of the Appendix. Case 1, 7, and 14 are selected as the sample represent all ranges of chimney diameter, chimney height and heat load as specified in Section Table 4. The contours for pressure, temperature, and velocity profile for Cases 1, 7 and 14 are shown in Figures 8 to 16.

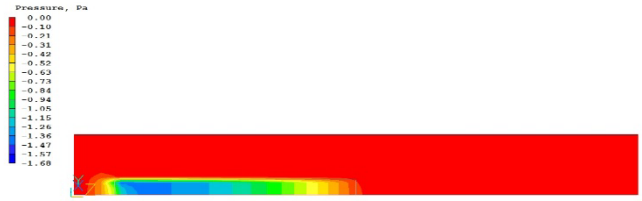

Figure 8. Plume pressure longitudinal (z) profile of Case 1.

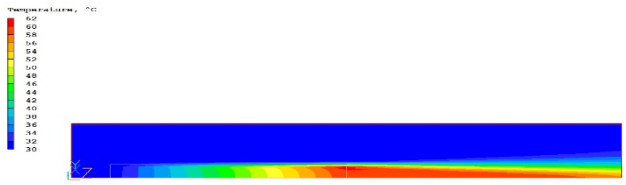

Figure 9. Plume temperature longitudinal (z) profile of Case 1.

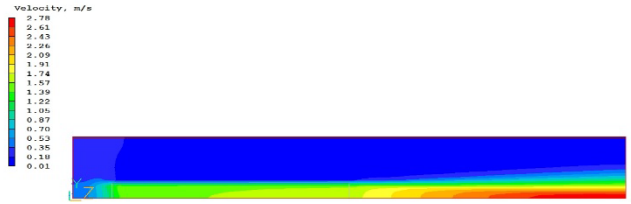

Figure 10. Plume velocity longitudinal (z) profile of Case 1.

Figure 11. Plume pressure longitudinal (z) profile of Case 7.

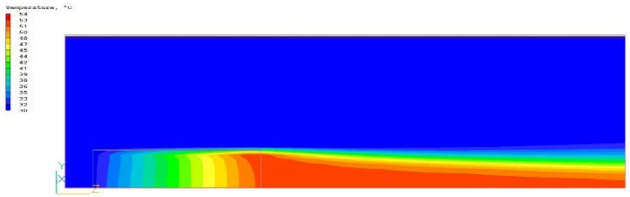

Figure 12. Plume temperature longitudinal (z) profile of Case 7.

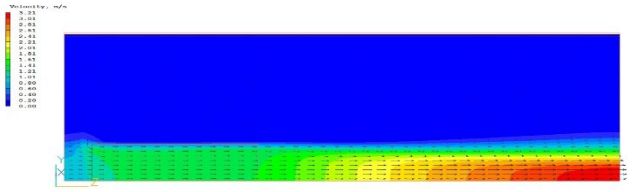

Figure 13. Plume Velocity Longitudinal (z) Profile of Case 7.

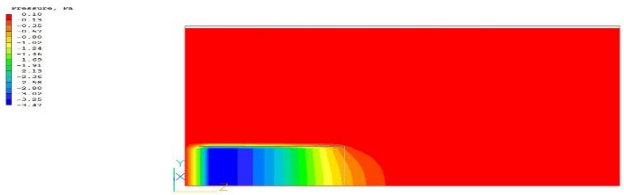

Figure 14. Plume pressure longitudinal (z) profile of Case 14.

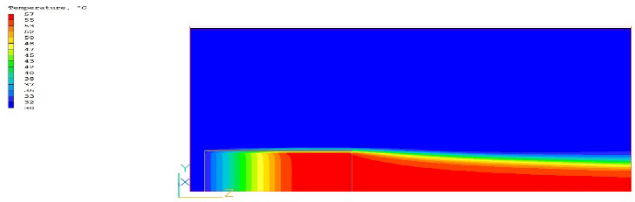

Figure 15. Plume temperature longitudinal (z) profile of Case 14.

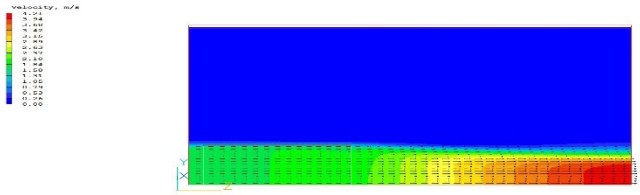

Figure 16. Plume velocity longitudinal (z) profile of Case 14.

4. RESULTS AND DISCUSSION

4.1 PVT Contour Plots

Three selected cases 1, 7 and 14 covering the full range of Richardson number are presented in Figures 8 to 16 the centre-plane longitudinal profiles of pressure, velocity and temperature. These plots reveal that the flow inside the vertical cylinders were generally one dimensional as expected of chimneys without any cold inflow, as the temperature contour plots show no deterioration of temperature at the point of the cylinder exit and in fact, appears to persist for a considerable distance downstream of the outlet, as it transitions from a lazy plume to pure plume flow. The simple average and trapezium-rule averaged density inside the cylinders also testify to a linear one-dimensional flow inside the cylinder. The simplifications in Section 3.3 appear to be acceptable.

Table 5. Plume function for each case.

Case	Source Richardson number, Ri_0	Plume function, Γ_0	Case	Source Richardson number, Ri_0	Plume function, Γ_0
1	0.046	1.04	9	0.200	4.40
2	0.034	1.01	10	0.140	3.10
3	0.097	2.12	11	0.140	3.12
4	0.070	1.51	12	0.079	1.73
5	0.039	1.08	13	0.330	7.13
6	0.039	1.09	14	0.330	7.16
7	0.200	4.32	15	0.220	4.78
8	0.200	4.36	16	0.220	4.80

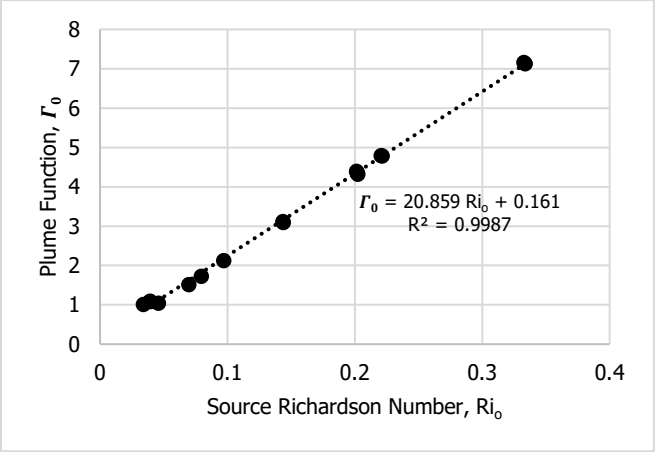

Figure 17. Graph of plume function against source Richardson number.

4.2 Plume Function

The source plume function and Richardson number for each case are determined using Equations (2) and (4) respectively. The plume function is highly dependent on the source Richardson number where the higher was the source Richardson number, the higher was the plume function. The results are tabulated in Table 5. The plume function of each scenario ranges between 1.01 to 7.16 with a source Richardson number ranging between 0.034 to 0.330. Hence, all the plumes for all scenarios are considered as lazy plumes as $\Gamma_0 > 1$ [7]. The graph of source plume function against source Richardson number based on Table 5 is plotted as shown in Figure 17. The source plume function is linearly proportional to source Richardson number. This is not unexpected since they are both functions of buoyancy and velocity. Plume function is however, able to define a pure plume when its value falls below 1.0. The cases being studied are expected to behave as lazy plumes with a significant value of EPCH.

4.3 EPCH Determination

The parameters required to calculate the EPCH are extracted through Inform Statement 13 function containing internal programmable codes in Phoenics VR. The EPCH of each case is calculated by using Equations (6) – (11). The results are tabulated in Table 6. The graph of EPCH against source Richardson number based on Table 6 is plotted as shown in Figure 18. It can be seen from Figure 18, the EPCH increases proportionally with the source Richardson number, and is strongly related to its source radius, buoyancy relative to its momentum. Hence, the EPCH versus source Richardson number shows a strong linear correlation with the coefficient of determination, $R^2 = 0.8942$. The higher the Richardson number, the higher is the source buoyancy compared to its momentum, and therefore the stack effect as measured by EPCH should be higher. At very low Richardson number, the EPCH does not appear to be intercepting the *Y*-axis at zero, indicating that as long as there is buoyancy, indefinitely increasing the momentum does not eliminate EPCH. The chimney wall effect should in fact be reinforced by higher momentum due to the slower radial penetration by entrainment.

The graph of EPCH against plume function based on Table 6 is plotted as shown in Figure 19. From Figure 19, the EPCH increases with the increase of the plume function. As again expected, the EPCH versus plume function shows a strong linear correlation with the coefficient of determination, $R^2 = 0.8933$, and that EPCH is strongly related to the source radius. By extending plume function to less than 1.0, i.e. forced plume region, it appears that the magnitude of EPCH still maintains a non-zero positive value. This suggest that in the force balance of jet propulsion, buoyancy effect should still be included in the analysis, in spite of its near-negligible magnitude. The good correlations of EPCH versus Richardson number and plume function mean that they can both be parameters to estimate EPCH.

Table 6. EPCH of each case.

Case	Source Richardson number, Ri_0	Plume function, Γ_0	EPCH, h_0 (m)	Case	Source Richardson number, Ri_0	Plume function, Γ_0	EPCH, h_0 (m)
1	0.046	1.04	0.495	9	0.200	4.40	0.951
2	0.034	1.01	0.506	10	0.140	3.10	1.018
3	0.097	2.12	0.674	11	0.140	3.12	0.975
4	0.070	1.51	0.691	12	0.079	1.73	0.890
5	0.039	1.08	0.645	13	0.330	7.13	1.671
6	0.039	1.09	0.607	14	0.330	7.16	1.604
7	0.200	4.32	1.053	15	0.220	4.78	1.447
8	0.200	4.36	0.993	16	0.220	4.80	1.409

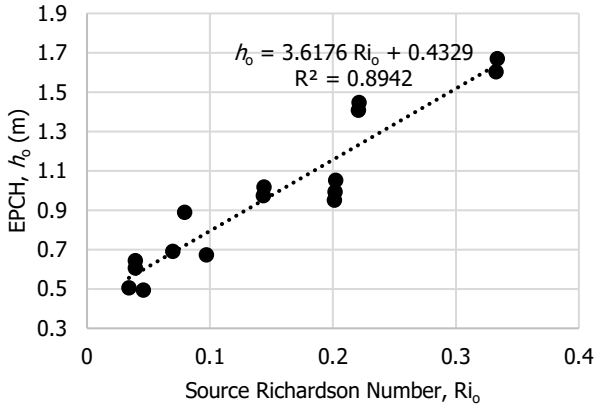

Figure 18. Graph of EPCH against source Richardson number.

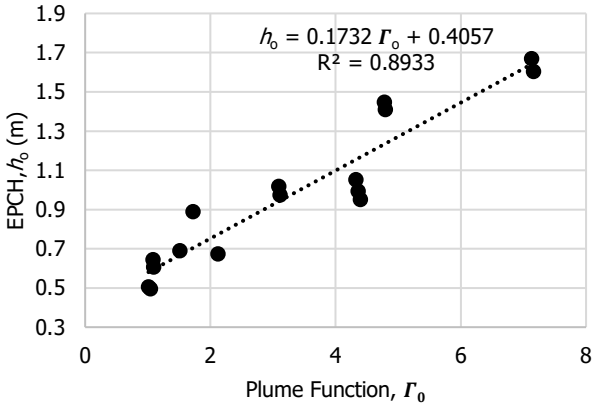

Figure 19. Graph of EPCH against plume function.

4.4 Determination of Coefficients of EPCH Correlation

The EPCH is here correlated with the same physical parameters as in [25] namely: diameter, d; volumetric coefficient of expansion of air, β; temperature differences between exit air and ambient air, ΔT; density of heated air, ρ_o; density difference between heated and ambient air, $\rho_a - \rho_o$. The parameters not included in the correlation were dynamic viscosity, η_o and gravitational constant, g; since they were held constant for all 16 cases. The EPCH correlation data are extracted from CFD simulation results and tabulated in Table 7.

The formulation of EPCH correlations is determined by Microsoft Excel. To use this function, the based-10 logarithms of all parameters in Table 8 were applied to the data in order to linearise the form of equation and they are tabulated in Table 8. The coefficients of EPCH correlation were then determined through Microsoft Excel Data Analysis Package Regression method. The EPCH shows a very strong correlation with the coefficient of determination, R^2 = 0.9999, Fisher F-ratio of 3412552, and the p-value of each parameter was much less than 0.05 except the coefficient of volumetric expansion at 0.06 and average outlet face velocity at 0.058. However, the velocity's index was found to be -0.00284 which is negligible. The correlation's predictions were virtually identical with data from CFD. The formula of EPCH correlations is shown in Equation (12):

$$h_o = 0.23 \frac{d^{0.5} \beta^{0.45} \Delta T^{0.80} \rho_o^{1.07}}{(\rho_a - \rho_o)^{0.97}} \tag{12}$$

The formula found as shown in Equation (12) indicates that EPCH is related to diameter of the chimney, $h_o \propto d^{0.5}$, as first predicted in [15] by a dimensional analysis, coincides with equations in [13][25][26]; it is dependence on temperature differences $h_o \propto \Delta T^{0.80}$, and on density difference of air between ambient and plume source, $h_o \propto (\rho_a - \rho_o)^{-0.97}$ also agrees with Chu1 equation [22]. The rest of the parameters however differ from all other models, namely, volumetric coefficient of expansion, $h_o \propto \beta^{0.45}$ and mean density of plume source, $h_o \propto \rho_o^{1.07}$. The omission of dynamic viscosity and gravitational acceleration constant from the correlation had not affected the basic trends of the parameters. However, the formula shows no correlation between average outlet velocity of the air and EPCH, which ranged from 1.33 to 2.67 ms^{-1}, in spite of a ratio of 1.93 between the maximum and the minimum. Besides, the ranges of variables for the correlation were not well distributed as shown in Table 9, in spite of a ratio of almost 10 between the maximum and minimum Richardson number, and β and ρ_o were both operating in narrow ranges. Though the indices of β and ρ_o differ from that of [25], but the sum of these indices appear to equal 1.50 for both equations, suggesting a minor difference in the models.

Table 7. EPCH correlation data of each case.

Case	h_o	d	$\beta \times 10^3$	ΔT	ρ_o	$\rho_a - \rho_o$	u	$\eta_o \times 10^5$	g
1	0.495	0.5	3.01	29.56	1.112	0.054	1.47	2	9.81
2	0.506	0.5	3.03	26.61	1.117	0.049	1.78	2	9.81
3	0.674	1.0	2.95	35.40	1.102	0.064	1.54	2	9.81
4	0.691	1.0	2.99	31.43	1.109	0.058	1.73	2	9.81
5	0.645	1.0	3.05	24.60	1.115	0.051	2.39	2	9.81
6	0.607	1.0	2.98	32.73	1.099	0.067	2.57	2	9.81
7	1.053	2.0	3.08	22.00	1.126	0.041	1.33	2	9.81
8	0.993	2.0	3.01	29.23	1.113	0.054	1.40	2	9.81
9	0.951	2.0	2.95	35.84	1.101	0.065	1.52	2	9.81
10	1.018	2.0	3.04	25.94	1.119	0.048	1.57	2	9.81
11	0.975	2.0	2.99	31.76	1.108	0.058	1.71	2	9.81
12	0.890	2.0	3.01	28.95	1.107	0.059	2.57	2	9.81
13	1.671	5.0	3.08	21.61	1.126	0.040	1.51	2	9.81
14	1.604	5.0	3.03	26.41	1.118	0.049	1.65	2	9.81
15	1.447	5.0	3.04	25.75	1.113	0.053	2.29	2	9.81
16	1.409	5.0	3.01	29.25	1.107	0.060	2.45	2	9.81

Table 8. Based-10 logarithms of EPCH correlations of each case.

Case	$\log(h_o)$	$\log(d)$	$\log(\beta)$	$\log(\Delta T)$	$\log(\rho_o)$	$\log(\rho_a - \rho_o)$
1	-0.3051	-0.301	-2.5221	1.4707	0.0462	-1.2656
2	-0.2958	-0.310	-2.5182	1.4250	0.0482	-1.3091
3	-0.1714	0	-2.5296	1.5490	0.0422	-1.1912
4	-0.1605	0	-2.5245	1.4974	0.0449	-1.2401
5	-0.1904	0	-2.5155	1.3909	0.0474	-1.2910
6	-0.2165	0	-2.5262	1.5149	0.0411	-1.1731
7	0.0223	0.301	-2.5121	1.3424	0.0514	-1.3886
8	-0.0029	0.301	-2.5216	1.4658	0.0464	-1.2702
9	-0.0218	0.301	-2.5302	1.5544	0.0419	-1.1861
10	0.0079	0.301	-2.5173	1.4139	0.0487	-1.3198
11	-0.0110	0.301	-2.5249	1.5019	0.0447	-1.2358
12	-0.0508	0.301	-2.5213	1.4617	0.442	-1.2272
13	0.2229	0.699	-2.5116	1.3347	0.0517	-1.3962
14	0.2051	0.699	-2.5179	1.4218	0.0483	-1.3124
15	0.1606	0.699	-2.5171	1.4108	0.0467	-1.2771
16	0.1491	0.699	-2.5217	1.4662	0.0441	-1.2244

Table 9. Magnitude of the range of each variable for correlation.

Ratio between maximum and minimum							
Diameter	Velocity	ΔT	$\Delta\rho$	β	ρ_o	Ri_o	Γ_o
10.00	1.94	1.66	1.67	1.04	1.03	9.82	7.08

4.5 Comparison with Doyle and Benkly [13] and Chu1 [25]

The EPCH measured from CFD Doyle and Benkly's [13] equation was designed for induced draft air-cooled heat exchangers which includes a step of estimating the face velocity by inputting the tube bundle number of rows and chimney height before evaluating the EPCH. Since the cylinder chimney here had no tube bundle, this was adapted to calculate the EPCH by using the CFD's average outlet velocity as an input rather than estimating it from their equation. Chu1 [25] and Chu2 [26] based on Chilton-Colburn are shown in Table 10.

The results of equations from [25] and [13] are plotted against the CFD measured EPCH in Figure 20 and the correlation by applying linear least-squares regression show Chu1 [25] equation to be strongly correlated with a standard error of 2.6% while Doyle and Benkly's [13] correlation is good with a standard error of 13.3 per cent, and Chu2 [26] equation based on Chilton-Colburn analogy was underpredicting the EPCH by about 60% with a standard error of 58.3%. The model based on the concept of analogy appears to breakdown with this set of data. The EPCH correlation formula found (after this known as "current method") is compared with EPCH correlation of [13] and [25]. If the parameters involving ΔT had been merged with $\Delta\rho$, the correlation would not fit that well, perhaps because the $\Delta\rho$ was to account for trace amount of compressibility in the buoyancy factor.

Table 10. Predicted EPCH of three methods vs measured EPCH-CFD.

Case	Ri_0	Γ_0	EPCH Measured from CFD	Doyle and Benkly [13]	Chu1 [25]	Chu2 [26]
1	0.046	1.04	0.495	0.436	0.507	0.200
2	0.034	1.01	0.506	0.445	0.521	0.203
3	0.097	2.12	0.674	0.652	0.684	0.276
4	0.070	1.51	0.691	0.651	0.705	0.280
5	0.039	1.08	0.645	0.664	0.666	0.290
6	0.039	1.09	0.607	0.726	0.619	0.279
7	0.200	4.32	1.053	0.788	1.093	0.417
8	0.200	4.36	0.993	0.857	1.016	0.400
9	0.200	4.40	0.951	0.921	0.964	0.389
10	0.140	3.1	1.018	0.857	1.048	0.407
11	0.140	3.12	0.975	0.921	0.995	0.396
12	0.079	1.73	0.890	0.996	0.911	0.401
13	0.330	7.13	1.671	1.282	1.735	0.660
14	0.330	7.16	1.604	1.378	1.650	0.642
15	0.220	4.78	1.447	1.487	1.490	0.645
16	0.220	4.80	1.409	1.56	1.442	0.634

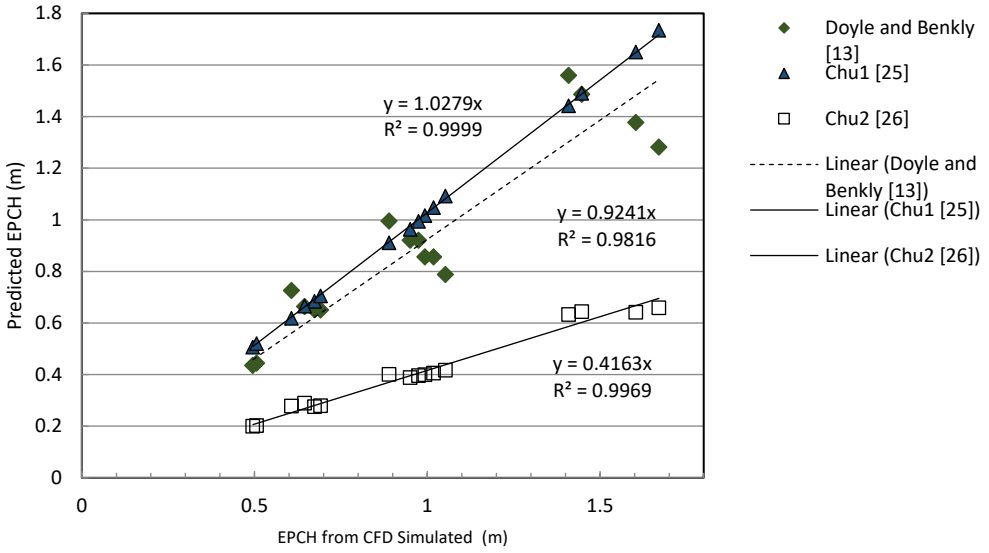

Figure 20. Correlation between EPCH from CFD and EPCH predicted.

The graph of EPCH of three methods against source Richardson number and EPCH of three methods against plume function based on Table 10 are plotted as shown in Figure 21 and Figure 22 respectively. From Figure 21, the trendline using all three methods show a very similar gradient against source Richardson number. EPCH estimated from Doyle and Benkly's [13] method has greater scatter than the current method and Chu1 [25]. A very close and similar trendline is achieved by using current method and Chu1 [25]. However, the EPCH estimated through Chu1 [25] is slightly greater than current method with the increases in source Richardson number. Similar to the plot of EPCH against source Richardson number in Figure 21, Figure 22 shows the trend lines of all three methods exhibit similar positive gradient against plume function, which is to be expected since the correlation coefficient between source Richardson number and source plume function is almost 1.0 (Figure 17).

All methods show upward trends with respect to Richardson number and Plume Function, as expected. Source Richardson number and Plume Function can also be used to correlate EPCH and since they are physically based should provide confidence over a wide range of conditions, but they lack agility in modelling the plume. The main finding from this CFD correlation is that EPCH depends on source diameter, temperature difference, and density significantly, with the index of diameter confirmed by all methods including the current method to be at 0.5, as predicted by Morton *et al.* [15] that characteristic heights of plumes are proportional to the square root of diameter, or to the $1/4^{th}$ power of the buoyancy flux. As shown in Table 9, the ranges of variables in future analysis should be sufficiently large to enable reaching meaningful correlation.

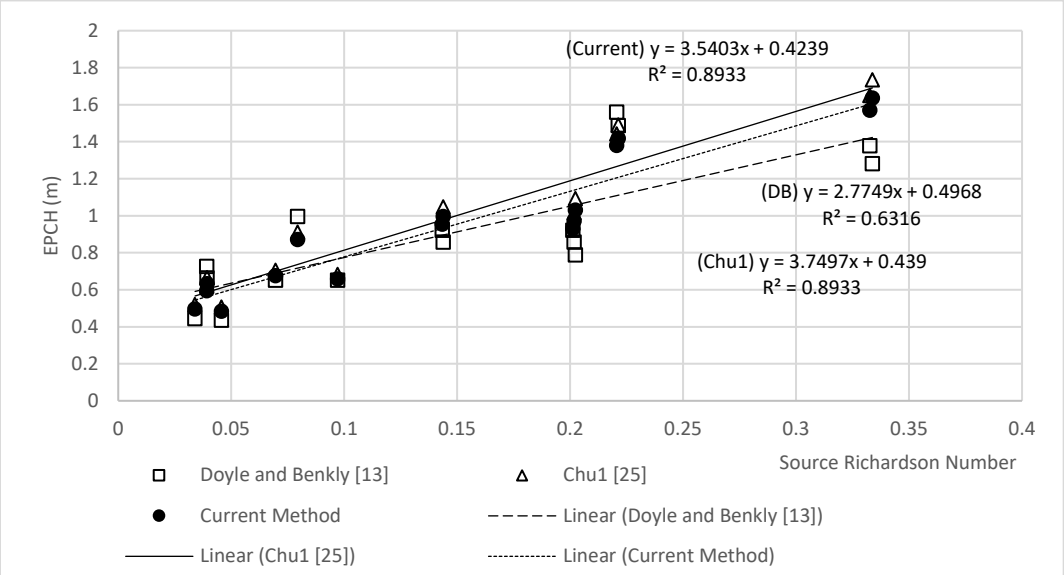

Figure 21. Graph of EPCH against source Richardson number for current method and Chu1 and DB methods.

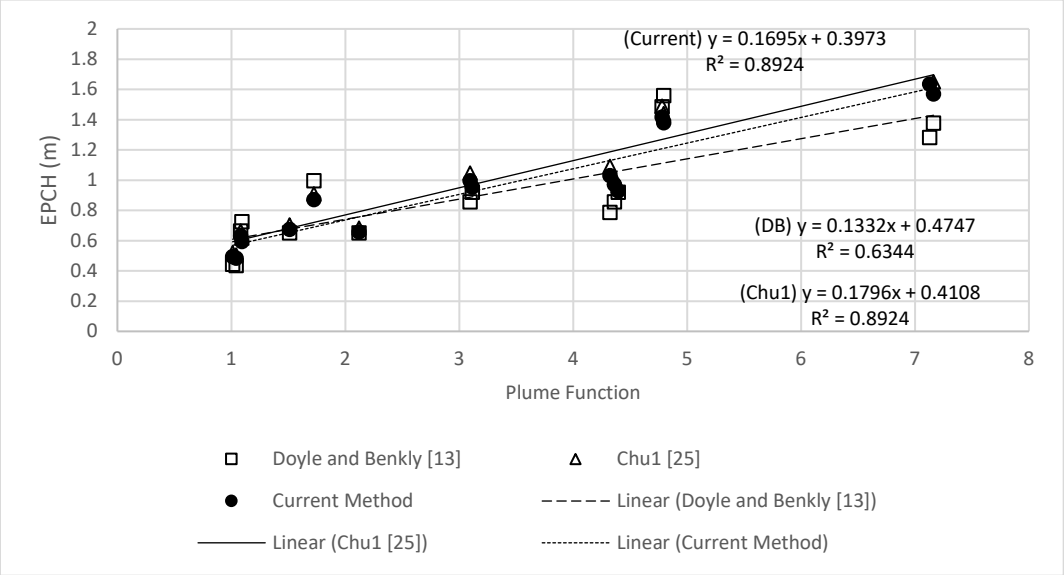

Figure 22. Graph of EPCH against plume function for current method and Chu1 and DB methods.

A characteristic of plume-chimney that may be a contributing factor to the so-called CAT [1] can be seen in Figure 23, a zone in a developing plume termed by Chen and Nikitopolous [33] as the zone of flow establishment (ZFE), at the point where the pure plume Gaussian profile begins to apply. Kuchimachi and Depopam's [8] experimental data using helium-air yielded this height as 3 times the source radius. Ciriello and Hunt [10] derived analytically for general cases this length, or the virtual origin correction length (VOCL) or height as 3.34 times of top-hat source radius, while Henderson-Sellors [34] gave this value as 8 times of source radius but Case 14 here appears to indicate this height to be at 12 times the source radius, since the decay of velocity must occur before a pure plume can emerge. The vast difference can be attributed to the ranges of plume source functions, where Kuchimachi and Depopam [8] set it at 2267, Kaye and Hunt [9] at between 9.1×10^4 and 5.4×10^7, and that of this study ranged from 1.01 to 7.16, which fell within the range of Marjanovic *et al.*'s [11] DNS simulation range of 1.06 to 424. The description of virtual origin correction in [10] equates the VOCL to the ZFE. Marjanovic *et al.* [11] compared their DNS observation by the behaviour of entrainment coefficient that the transition from lazy plume to pure plume occurred at only after 40 plume radii, against Carlotti and Hunt's [12] theoretical model of entrainment that predicts very rapid decay to far-field behaviour (less than 10 plume source radii). Marjanovic *et al.*'s [11] predicted point of transition to pure plume are at the same order of magnitude of ZFE for case 14 in this study (Figure 23). This zone can be a potent source of updraft turbulence with the plume behaving as a chimney that preserves thermal energy or buoyancy collectively due to its invisible wall.

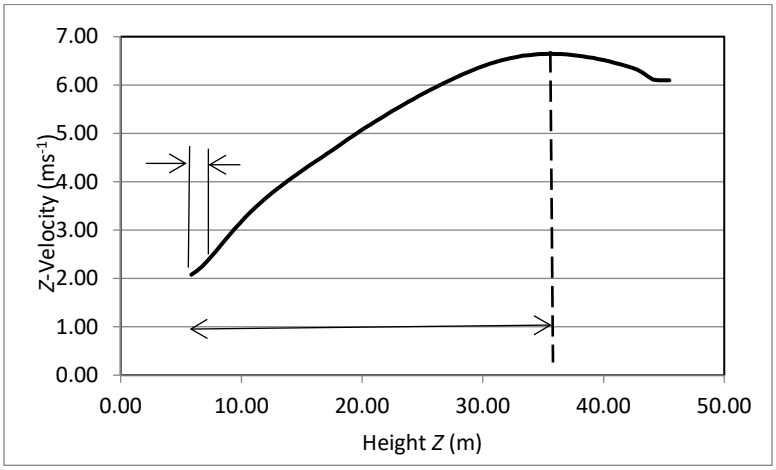

Figure 23. Vertical axial velocity versus vertical height for Case 14.

The plume chimney can form in perfectly calm conditions and with a source diameter of 60 km, an ocean seawater temperature of mere 27°C and ambient air temperature of 15°C. It is estimated the vertical velocity could reach a minimum of 8 ms^{-1} or 30 km/hr at about 5.3 km height, based on the integral model for hurricane "Hot Towers" described in [35]. The height to source radius ratios for VOCL or ZFE prediction are perhaps too simplistic for scaling as a lazy plume source diameter of a mere 1 km could yield a ZFE of 1.5 to 20 km. However, from the CFD analysis of lazy plume above, in confirming the dimensional analysis of Morton *et al.* [15], the ratio of $h_2/h_1 \propto (D_2/D_1)^{1/2}$ may be a better scaling formula for extrapolating characteristic heights of plume, and ignoring the air density changes with height, a source diameter of 60 km (D_2) would give rise to a ZFE of 4 km, scaled up from the ZFE of case 14 (D_1), within an order of magnitude estimated using the integral model. This ZFE or VOCL is capable of reaching 5.6 km height in the troposphere which is defined by Ellrod *et al.* [1] as the height above which CAT occurs, and it is becoming an aviation safety risk is not unrealistic since 30 km/hr of updraft wind is not insignificant. This hypothesis may add a piece to the CAT puzzle among other atmospheric turbulences like thermal convection and mountain waves.

5. CONCLUSION

In conclusion, an effective plume-chimney height (EPCH) correlation was derived from the CFD simulation results using Phoenics VR. EPCH was obtained from CFD results via a zero-gravity method of measuring the total pressure drop. EPCH is correlated with buoyancy of the air and the dimension of the models (in this case diameter). It was found that EPCH was not insignificant but dependent on:

a) The diameter of the chimney with $h_o \propto d^{0.5}$, in line with the prediction through dimensional analysis by Morton *et al.* [15] and all existing EPCH methods.
b) Volumetric coefficient of expansion with $h_o \propto \beta^{0.45}$.
c) Temperature difference, with $h_o \propto \Delta T^{0.80}$.
d) Mean density of plume source, with $h_o \propto \rho_o^{1.08}$.
e) Density difference of air between ambient and plume source, with $h_o \propto (\rho_a - \rho_o)^{-0.97}$.
f) The correlation with the velocity of the air was negligible.

Apart from diameter, velocity and temperature difference, the ranges of the other parameters were not wide enough for the correlation to be meaningful. It is proposed that the $h_o \propto d^{0.5}$ relationship be extended to apply as a scaling formula to plume characteristic heights.

EPCH was also found to have a strong, positive, linear correlation with both Richardson number and plume function. The correlation developed using the current method of analysis was found to be very close to the existing Chu1 [25] having similar parameters but Chu2 [26] method which was based on Chilton-Colburn analogy was shown to breakdown. The current method also has a similar trend to Doyle and Benkly [13] method and have less scatter overall at the same Richardson number and plume function.This CFD evidence of the existence of a plume-chimney that conserves buoyancy to rise and attain high axial vertical updraft velocity to heights where CAT are detected and experienced, severely affecting the safety of flights, suggests further investigation by CFD or field measurements of pockets of mesoscale plumes will be beneficial to the aviation industry.

ACKNOWLEDGEMENT AND FUNDING

The authors would like to offer their sincere thanks to the Ministry of Higher Education, Malaysia, for the kind assistance provided through fundamental grants No. FRG0022 and FRG0197 and the provision of funding the CFD licence by Universiti Malaysia Sabah under SGA0034.

DECLARATION OF CONFLICTING INTERESTS

The authors declare no potential conflicts of interest with respect to the research and publication of this article.

REFERENCES

[1] G.P. Ellrod, J. A. Knox, P. F. Lester and L. J. Ehernberger, Clear air turbulence, aviation meteorology-clear air turbulence, *Encyclopedia of Atmospheric Sciences 2nd Edition*, 2015, 1, 177-186.

[2] L. N. Storer, P. D. Williams and M. M. Joshi, Global response of clear-air turbulence to climate change, *Geophysical Research Letters*, 2017, 44, 9976-9984.

[3] D. W. Saxton, The nature and causes of clear-air turbulence, *Journal of Aircraft*, 4(4), 1967, July, 356,

[4] P.F. Crapper, Forced plume characteristics, *Tellus*, 29(5), 1977, 470-475.

[5] P. Zannetti, Gaussian models, *Air Pollution Modelling*, Springer: Boston, USA, 1990.

[6] G. Marjanovic, G. Taub and S. Balachander, On the effects of buoyancy on higher order moments in lazy plumes, *Journal of Turbulence*, 20(2), 2018, 121-146.

[7] C. P. Caulfield and A. W. Woods, Plumes with non-monotonic mixing behaviour, *Geophysical & Astrophysical Fluid Dynamics,* 79, 1995, 173-199.

[8] K. B. Kuchimanchi and D. Depopam, Experimental Investigation of a turbulent lazy plume, *INCOM18: Proceedings of 1st International Conference on Mechanical Engineering,* Kolkata, India, 2018, 250.

[9] N. B. Kaye and G. R. Hunt, An experimental study of large area source turbulent plumes, *International Journal. of Heat and Fluid Flow*, 30, 2009, 1099-1105.

[10] F. Ciriello and G. R. Hunt, Analytical solutions and virtual origin corrections for forced, pure and lazy turbulent plumes based on a universal entrainment function, *Journal of Fluid Mechanics,* 893, 2020, A12.

[11] G. Marjanovic, G. N. Taub and S. Balachandar, On the evolution of the plume function and entrainment in the near-source region of lazy plumes, *Journal of Fluid Mechanics*, 830, 2017, 736-759.

[12] P. Carlotti and G. R. Hunt, An entrainment model for lazy turbulent plumes, *Journal of Fluid Mechanics*, 11, 2017, 682-700.

[13] P. T. Doyle and G. J. Benkly, Use fanless air coolers, *Hydrocarbon Processing*, 1973, 81-86.

[14] S. H. Kim, J. H. Kim, H. Y. Chun and R. D. Sharm, Global response of upper-level aviation turbulence from various sources to climate change, *Climatic Atmospheric Science,* 6, 2023, 92.

[15] B. R. Morton, G. I. Taylor and J.S. Turner, Turbulent gravitational convection from maintained and instantaneous sources, *Proceedings of Royal Society London*, A234, 1956, 1-23.

[16] B. R. Morton, Forced plumes, *Journal of Fluid Mechanics*, 5, 1959, 151-163.

[17] B. R. Morton, and J. Middleton, Scale diagrams for forced plumes, *Journal of Fluid Mechanics*, 58, 1973, 165-176.

[18] E. J. List and J. Imberger, Turbulent entrainment in buoyant jets and plumes, *Journal of Hydraulics Division*, 99, 1973, 1461-1474.

[19] G. S. Bhat and R. Narasimha, A volumetrically heated jet: Large-eddy structure and entrainment characteristics, *Journal of Fluid Mechanics*, 325, 1996, 303-330.

[20] K. R. Sreenivas and A. K. Prasad, Vortex-dynamics model for entrainment in jets and plumes, *Physics of Fluids*, 12, 2000, 2101-2107.

[21] E. Kaminski, S. Tait, and G. Carazzo, Turbulent Entrainment in jets with arbitrary buoyancy, *Journal of Fluid Mechanics*, 526, 2005, 361-376.

[22] M. Van Reeuwijk and J. Craske, Energy-consistent entrainment relations for jets and plumes, *Journal of Fluid Mechanics*, 782, 2015, 333-355.

[23] G. R. Hunt and N. B. Kaye, Lazy plumes*, Journal of Fluid Mechanics*, 553, 2005, 329-338.

[24] G. Carazzo, E. Carazzo, E. Kaminski and S. Tait, On the rise of turbulent plumes: Quantitative effects of variable entrainment for submarine hydrothermal vents, terrestrial and extra terrestrial explosive volcanism, *Journal of Geophysical Research*, 113, 2008, 1-19.

[25] C. -M. Chu, A preliminary method for estimating the effective plume chimney height above a forced-draft air-cooled heat exchanger operating under natural convection, *Heat Transfer Engineering*, 23, 2002, 3-12.

[26] C. -M. Chu, Use of Chilton-Colburn analogy to estimate effective plume chimney height of a forced draft, air-cooled heat exchanger, *Heat Transfer Engineering*, 27(9), 2006, 81-85.

[27] C. -M. Chu, Lazy plume stack effect above chimney, *Cold Inflow-Free Solar Chimney*, Singapore: Springer, 2021, 75-102

[28] X. X. Li, S. Duniam, H. Gurgenci, Z. Q. Guan and A. Veeraragavan, Full scale experimental study of a small natural draft dry cooling tower for concentrating solar thermal power plant, *Applied Energy,* 193, 2017, 15-27.

[29] S. E. Haaland, Simple and explicit formulas for the friction factor in turbulent pipe flow, *Journal of Fluids Engineering*, 105(1), 1983, 83-90.

[30] ASHRAE, *ASHRAE Handbook- Fundamentals*, 2017.

[31] Y. S. Chen and S. W. Kim, *Computation of Turbulent Flows using an Extended K-E Turbulence Closure Model*, NASA CR-179204, 1987.

[32] H. Nakagome and M. Hirata, The structure of turbulent diffusion in an axi-symmetrical thermal plume, *Proceedings of International Center for Heat and Mass Transfer, Seminar on Turbulent Buoyant Convection*, Dubrovnik, Yugoslavia, 1976, 365-372.

[33] C. J. Chen and C. P. Nikitopoulos, On the near field characteristics of axisymmetric turbulent buoyant jets in uniform environment, *International Journal of Heat and Mass Transfer*, 22, 1979, 245-255.

[34] B. Henderson-Sellers, The zone of flow establishment for plumes with significant buoyancy, *Applied Mathematical Modelling*, 7, 1983, 396-398.

[35] C. -M. Chu, Hot towers formation – a simple integral model of plume rise, *Conference on Hurricanes and Tropical Meteorology*, Orlando, USA, 2008.

NOMENCLATURE

A_F	Bundle face area	(m^2)
c_p	Specific heat capacity of air	$(\mathrm{Jkg}^{-1}\mathrm{K}^{-1})$
d	Diameter of chimney	(m)
D_H	Hydraulic diameter	(m)
F_0	Buoyancy flux	$(\mathrm{m}^4\mathrm{s}^{-3})$
g	Gravitational constant	(ms^{-2})
Gr	Grashof number	$(-)$
h_0	Effective plume-chimney height	(m)
h_{sw}	Height of solid walled chimney	(m)
L	Horizontal square flat plate length	(m)
L_B	Bundle breath	(m)
L_T	Bundle length	(m)
M_0	Momentum flux	$(\mathrm{m}^4\mathrm{s}^{-2})$
$\mathrm{N_R}$	Number of tube rows	$(-)$
P_{wall}	Solid walled buoyant pressure	(Pa)
P_{fixed}	Fixed buoyant pressure	(Pa)
Pr	Prandtl number	$(-)$
Q_0	Mass flux	$(\mathrm{kgm}^{-2}\mathrm{s}^{-1})$
R	Universal gas constant	$(\mathrm{Jkg}^{-1}\mathrm{K}^{-1})$
Ri_0	Source Richardson number	$(-)$
r	Plume radius	(m)
T_0	Ambient temperature	(K)
T_i	Initial temperature	(K)
T_{pi}	Process inlet temperature	(K)
u	Mean vertical velocity	(ms^{-1})
u_F	Face velocity	(ms^{-1})
z	Vertical height from plume source	(m)

Greek Symbol

α	Entrainment coefficient	$(-)$
β	Volumetric coefficient of expansion	(K^{-1})
Δp_{pipe}	Pressure drops due to pipe wall friction	(Pa)
Δp_{inlet}	Pressure drops due to pipe inlet entrance	(Pa)
Δp_{outlet}	Pipe outlet pressure drop	(Pa)
$\Delta p_{compressor}$	Available compressor pressure head	(Pa)
ΔT	Temperature difference between ambient and exit air	(K)
Γ_0	Plume source function	$(-)$
ρ_a	Density of ambient air	(kgm^{-3})
ρ_{av}	Average density of heated air	(kgm^{-3})
ρ_0	Mean density of plume source	(kgm^{-3})
η_0	Dynamic viscosity	(Nsm^{-2})
λ	Thermal conductivity	$(\mathrm{Wm}^{-2}\mathrm{K}^{-1})$

APPENDIX

Table A1: Structured mesh grid optimization for each case.

Case	Mesh grid density by number of cells in region	Case	Mesh grid density by number of cells in region
1	*X*: 1; *Y*: 2, 36; *Z*: 2, 1, 2, 1, 2, 1, 1, 2, 1, 2, 1, 30, 23.	9	*X*: 1; *Y*: 4, 36; *Z*: 2, 1, 2, 1, 2, 1, 1, 2, 1, 2, 1, 30, 23.
2	*X*: 1; *Y*: 4, 36; *Z*: 2, 2, 2, 2, 2, 2, 2, 2, 2, 2, 2, 2, 30, 26.	10	*X*: 1; *Y*: 4, 36; *Z*: 2, 2, 2, 2, 2, 2, 2, 2, 2, 2, 2, 2, 30, 26.
3	*X*: 1; *Y*: 4, 36; *Z*: 2, 1, 2, 1, 2, 1, 1, 2, 1, 2, 1, 30, 23.	11	*X*: 1; *Y*: 4, 36; *Z*: 2, 2, 2, 2, 2, 2, 2, 2, 2, 2, 2, 2, 30, 26.
4	*X*: 1; *Y*: 4, 36; *Z*: 2, 2, 2, 2, 2, 2, 2, 2, 2, 2, 2, 2, 30, 26.	12	*X*: 1; *Y*: 4, 36; *Z*: 3, 4, 3, 4, 3, 4, 3, 4, 3, 4, 3, 17, 14.
5	*X*: 1; *Y*: 4, 36; *Z*: 4, 4, 4, 4, 4, 3, 4, 4, 4, 4, 4, 17, 20.	13	*X*: 1; *Y*: 4, 36; *Z*: 2, 2, 2, 2, 2, 2, 2, 2, 2, 2, 2, 30, 26.
6	*X*: 1; *Y*: 4, 36; *Z*: 4, 4, 4, 4, 4, 3, 4, 4, 4, 4, 4, 17, 20.	14	*X*: 1; *Y*: 4, 36; *Z*: 2, 2, 2, 2, 2, 2, 2, 2, 2, 2, 2, 30, 26.
7	*X*: 1; *Y*: 4, 36; *Z*: 2, 1, 2, 1, 2, 1, 1, 2, 1, 2, 1, 30, 23.	15	*X*: 1; *Y*: 4, 36; *Z*: 3, 4, 3, 4, 3, 4, 3, 4, 3, 4, 3, 17, 14.
8	*X*: 1; *Y*: 4, 36; *Z*: 2, 1, 2, 1, 2, 1, 1, 2, 1, 2, 1, 30, 23.	16	*X*: 1; *Y*: 4, 36; *Z*: 3, 4, 3, 4, 3, 4, 3, 4, 3, 4, 3, 17, 14.